Acta Geod Geophys (2017) 52:375–388
DOI 10.1007/s40328-016-0175-3

ORIGINAL STUDY

A modified un-combined model to improve the performance of precise point positioning: model and test results

Xingwang Zhao[1] · Chao Liu[1] · Jian Deng[2] · Cuiying Zhang[1] · Xuexiang Yu[1]

Received: 24 January 2016 / Accepted: 23 May 2016 / Published online: 6 June 2016

Abstract Precise point positioning (PPP) can achieve high-accuracy point solution using un-differenced code and carrier phase observations. Many PPP models have a higher measurement noise and multipath effects, resulting in a long time to obtain sub-decimeter to centimeter positioning accuracy during a short duration. This paper will address a modified un-combined (MUC) model based on phase–phase geometry-free combination in addition to code–phase ionosphere-free combination and original carrier phase observations. The observation system composed by the new combinations has a lower measurement noise and orbit error level compared with the un-combined (UC) model, University of Calgary (UofC) model and standard un-differenced ionosphere-free combined (UD) model. Moreover, it can capture the changing characteristics of atmospheric delays between epochs as constraints to accelerate the filter convergence. We use the data sets from about 114 international GNSS service reference stations to analyze the performance of the MUC model. Numerical results show that the MUC model generally yields the best performance when the observation duration is short. For the 0.5 h duration observation data sets, about 70.2 % of all 6912 convergence tests are convergent, which is an increase by 19.2, 2.8 and 49.3 % points compared with the UC, UofC and UD models, respectively. For the common convergence parts of all the test data sets, the mean convergence time of the MUC model is significantly reduced by 22.9, 9.6 and 35.3 %, and the percentage of the 2D position biases within 0–5 cm is increased by 16.0, 3.4 and 55.0 %, respectively, compared with the UC, UofC and UD models. Therefore, the proposed PPP model is more beneficial for the PPP user to quickly obtain sub-decimeter to centimeter positioning accuracy during a short duration.

✉ Xingwang Zhao
xwzhao2008@126.com

[1] School of Geodesy and Geomatics, Anhui University of Science and Technology, Huainan 232001, China

[2] School of Computer and Information Engineering, Xiamen University of Technology, Xiamen 361024, China

Keywords Precise point positioning · Functional model · Convergence time · Accuracy

1 Introduction

Precise point positioning (PPP) is a desirable GNSS positioning technology because it has the advantage of being highly accurate and it is not limited by the baseline length. PPP technology can achieve precise positioning at a global scale using a single receiver in combination with a precise clock, orbit and other precise products provided by organizations such as international GNSS service (IGS) (Zumbeger et al. 1997; Kouba and Heroux 2001). Therefore, it has been gradually used in precise positioning, satellite orbit determination, atmospheric water vapor detection and seismic wave detection (Zhang et al. 2013a; Ahmed et al. 2014; Xu et al. 2013). However, in practice, the long convergence time of the PPP technology is beyond the acceptance level of most users, which limits its application in more fields.

How to improve the PPP performance has attracted many researchers since PPP has been proposed. The performance of the PPP solution is affected by the number of visible satellites, data quality, potential error sources, especially ionospheric delay. In order to remove the ionosphere delay, a variety of PPP models have been proposed, such as the undifferenced ionosphere-free combined (UD) model (Kouba and Heroux 2001), the University of Calgary (UofC) model (Gao and Shen 2001), and the un-combined (UC) model (Zhang et al. 2010, 2012). The main difference of these models is about how to mitigate the ionospheric delays. The UD model has been derived for the first time based on the standard ionosphere-free code and phase combination observations (Kouba and Heroux 2001). Then Gao and Shen (2001) further proposed a UofC model that is composed of the phase and code–phase ionosphere-free observation combinations, which has a smaller measurement noise level compared with the standard ionosphere-free code combination. However, although the ionosphere-free combination observation can remove the ionospheric delay, the measurement noise and multipath effects are amplified, which prohibits fast convergence of PPP ambiguity. Hence, in order to lower the measurement noise and multipath effects, an UC model was derived based on original code and carrier phase observations (Zhang et al. 2010), which mitigates the impact of the ionospheric delay by parameter estimation. A detailed comparison and analysis of these models is presented in the literature (e.g., Zhang et al. 2013b; Zhao et al. 2014).

In addition, some achievements have been also made to accelerate the convergence speed of PPP solution. On one hand, we can adopt augmented corrections (e.g., atmospheric delay and uncalibrated phase delay) to mitigate the potential error sources (Ge et al. 2008; Collins 2008; Laurichesse et al. 2009; Zhang et al. 2012; Shi et al. 2014), and improve the convergence speed of PPP solution (Geng et al. 2009; Collins et al. 2010; Li et al. 2013; Li et al. 2014a; Wen et al. 2015). On the other hand, the multi-GNSS systems can enhance the performance of GPS-only positioning by providing more redundent observations and improving satellite geometric strength (Moreno et al. 2014; Li and Zhang 2014; Li et al. 2014b). The positioning accuracy and convergence time can be improved based on the augmented corrections or the multi-GNSS PPP; nevertheless, we still need the three basic models mentioned above to obtain the PPP solutions. Although much effort has been made to improve the PPP performance, the PPP technique still suffers from a long convergence time of 30 min or more to obtain the required accuracy (less than 10 cm) with

an ambiguity-float solution or to succeed in an ambiguity-fixed solution (Bisnath and Gao 2009; Geng et al. 2011; Dawidowicz and Krzan 2014).

In view of the above, this paper presents a new model namely modified un-combined (MUC) model based on the existing research, which is suitable for a fast-PPP. The observation system of the MUC model consists of four observation equations: phase–phase geometry-free combination, code–phase ionosphere-free combination and two original carrier phase observations. This model has a smaller measurement noise and orbit error level compared with the UC, UofC and UD models. More importantly, the phase–phase geometry-free combinations are used in the observation system, which can improve the correlation between the estimated parameters over short observation periods.

Subsequently, the MUC model for a fast-PPP is first presented, and the differences between the MUC, UC, UofC and UD models are analyzed. Then, the experimental design and numerical results are described to assess the convergence performance as well as positioning accuracy in Sect. 3. Finally, the main conclusions are summarized in Sect. 4.

2 Mathematical models

2.1 Measurement equation

For a satellite s observed by a receiver, the original code and carrier phase observations can be expressed as follows:

$$\begin{cases} P_i^s = \rho_{\mathrm{r}}^s + c \cdot \delta t_{\mathrm{r}} - c \cdot \delta t^s + M_{\mathrm{d}}^s \cdot \delta_{\mathrm{zhd}} + M_{\mathrm{w}}^s \cdot \delta_{\mathrm{zwd}} + I_i^s + c(b_{\mathrm{r},i} - b_i^s) + \varepsilon_{\mathrm{P}_i^s} \\ \Phi_i^s = \rho_{\mathrm{r}}^s + c \cdot \delta t_{\mathrm{r}} - c \cdot \delta t^s + M_{\mathrm{d}}^s \cdot \delta_{\mathrm{zhd}} + M_w^s \cdot \delta_{\mathrm{zwd}} - I_i^s + \lambda_i(N_i^s + B_{\mathrm{r},i} + B_i^s) + \varepsilon_{\Phi_i^s} \end{cases} \quad (1)$$

where i the frequency of satellite signal, P_i^s, Φ_i^s the code and phase observations, ρ_{r}^s the geometrical distance between satellite and receiver, δt_{r} the receiver clock error, δt^s the satellite clock error, M_{d}^s, M_{w}^s the dry and wet tropospheric mapping functions, δ_{zhd}, δ_{zwd} the dry and wet zenith tropospheric delays, I_i^s the ionospheric delay, $b_{\mathrm{r},i}$, b_i^s the code hardware delay for receiver and satellite, $B_{\mathrm{r},i}$, B_i^s the carrier phase hardware delay for receiver and satellite, λ_i the wavelength, $\varepsilon_{\mathrm{P}_i^s}$, $\varepsilon_{\Phi_i^s}$ the sum of the multipath effects and measurement noises of the code and carrier phase observations.

Following the literature (Teunissen and Kleusberg 1996), the hardware delay biases for satellites and receiver will in general be different for different signal frequencies. Considering that the code hardware delay biases for satellites are contained in the precise clock products provided by IGS analysis centers. When using the IGS clock products, the code hardware delay biases for satellites can be removed in the PPP processing (Defraigne and Baire 2011). Assume that all hardware delay biases for receiver are constant over time (Teunissen and Kleusberg 1996; Ge et al. 2008). Thus, the carrier phase hardware delay biases for satellites and receiver can also be absorbed by the ambiguities, if they are not fixed to integers. And, the code hardware delay for receiver can be rewritten as a sum of a mean term and a frequency-dependent bias term as given below:

$$b_{\mathrm{r},i} = b_{\mathrm{r}}^{avg} + \delta b_{\mathrm{r},i} \quad (2)$$

where b_{r}^{avg} is the mean hardware delays for the code at receiver end, $\delta b_{r,i}$ is the frequency-dependent delay.

The mean code hardware delay bias can be assimilated into the receiver clock offset. Thus, by applying Eq. (2), the Eq. (1) can be rewritten as:

$$\begin{cases} P_{\mathrm{i}}^{s} = \rho_{\mathrm{r}}^{s} + c \cdot \delta\bar{t}_{\mathrm{r}} - c \cdot \delta\bar{t}^{s} + M_{\mathrm{d}}^{s} \cdot \delta_{\mathrm{zpd}} + M_{\mathrm{w}}^{s} \cdot \delta_{\mathrm{zpw}} + I_{\mathrm{i}}^{s} + \delta b_{\mathrm{r,i}} + \varepsilon_{\mathrm{P}_i^s} \\ \Phi_{\mathrm{i}}^{s} = \rho_{\mathrm{r}}^{s} + c \cdot \delta\bar{t}_{r} - c \cdot \delta\bar{t}^{s} + M_{\mathrm{d}}^{s} \cdot \delta_{\mathrm{zpd}} + M_{\mathrm{w}}^{s} \cdot \delta_{\mathrm{zpw}} - I_{\mathrm{i}}^{s} + \lambda_{\mathrm{i}}\bar{N}_{\mathrm{i}}^{s} + \varepsilon_{\Phi_i^s} \end{cases} \tag{3}$$

where $\delta\bar{t}_r^j$ and $\delta\bar{t}^s$ are the reformed receiver clock offset and satellite clock offset, respectively; $\bar{N}_i^s$ is the sum of the integer ambiguity and hardware delay biases, referred to as phase-biases. Hence:

$$\begin{cases} \delta\bar{t}_{\mathrm{r}} = \delta t_{\mathrm{r}} + b_{\mathrm{r}}^{avg} \\ \delta\bar{t}^{s} = \delta t^{s} + b_{\mathrm{i}}^{s} \\ \bar{N}_{\mathrm{i}}^{s} = N_{\mathrm{i}}^{s} + B_{\mathrm{r,i}} + B_{\mathrm{i}}^{s} - c \cdot (b_{\mathrm{r}}^{avg} - b_{\mathrm{i}}^{s})/\lambda_{\mathrm{i}}. \end{cases}$$

The term $\delta b_{\mathrm{r},i}$ in Eq. (3) can be estimated as frequency-dependent unknown parameters (Defraigne and Baire 2011). However, too many unknown parameters will weaken the model structure for PPP. Because of assigning a much smaller weight to the code observations in the PPP processing, the term $\delta b_{R,i}$ can be neglected and its effects will show up in the code residuals (Cai and Gao 2013; Zhao et al. 2016). Thus, the Eq. (3) can be rewritten as:

$$\begin{cases} \mathrm{P}_{\mathrm{i}}^{s} = \rho_{\mathrm{r}}^{s} + c \cdot \delta\bar{t}_{\mathrm{r}} - c \cdot \delta\bar{t}^{s} + M_{\mathrm{d}}^{s} \cdot \delta_{\mathrm{zpd}} + M_{\mathrm{w}}^{s} \cdot \delta_{\mathrm{zpw}} + I_{\mathrm{i}}^{s} + \varepsilon_{\mathrm{P}_i^s} \\ \Phi_{\mathrm{i}}^{s} = \rho_{\mathrm{r}}^{s} + c \cdot \delta\bar{t}_{\mathrm{r}} - c \cdot \delta\bar{t}^{s} + M_{\mathrm{d}}^{s} \cdot \delta_{\mathrm{zpd}} + M_{\mathrm{w}}^{s} \cdot \delta_{\mathrm{zpw}} - I_{\mathrm{i}}^{s} + \lambda_{\mathrm{i}}\bar{N}_{\mathrm{i}}^{s} + \varepsilon_{\Phi_i^s}. \end{cases} \tag{4}$$

The noise level reflects the accuracy of the observation system. To lower the code observation noise level, the code observation P_i^s and carrier phase observation Φ_i^s can be combined using the following equation:

$$\mathrm{L}_{\mathrm{P}_i^s\Phi_i^s}^{s} = \left(\mathrm{P}_i^s + \Phi_i^s\right)/2 = \rho_{\mathrm{r}}^{s} + c \cdot \delta\bar{t}_{\mathrm{r}} - c \cdot \delta\bar{t}^{s} + M_{\mathrm{d}}^{s} \cdot \delta_{\mathrm{zpd}} + M_{\mathrm{w}}^{s} \cdot \delta_{\mathrm{zpw}} + \lambda_i\bar{N}_i^s/2 + \varepsilon_{\mathrm{L}_{\mathrm{P}_i^s\Phi_i^s}}. \tag{5}$$

Equation (5) is the so-called code–phase ionospheric-free combination that eliminates the ionospheric effect.

Moreover, a new phase–phase geometry-free combination is considered to strengthen the algebraic structure for PPP model, as shown in the following equation:

$$\Phi_{\mathrm{GF}}^{s} = \Phi_1^s - \Phi_2^s = -I_1^s + I_2^s + \lambda_1\bar{N}_1^s - \lambda_2\bar{N}_2^s + \varepsilon_{\Phi_{\mathrm{GF}}^s}. \tag{6}$$

It is obvious that the orbit error has been eliminated by the phase–phase geometry-free combination in Eq. (6). Moreover, the new combination has a smaller measurement noise level than the ionospheric-free combination or original code observation, which is beneficial to the PPP solution.

Subsequently, a new model is obtained based on the original carrier phase observations Φ_1^s, Φ_2^s in Eq. (4), code–phase ionospheric-free combinations $\mathrm{L}_{\mathrm{P}_i^s\Phi_i^s}^{s}$ in Eq. (5) and phase–phase geometry-free combination Φ_{GF}^{s} in Eq. (6). Note that the code–phase ionospheric-free combinations still have a higher measurement noise level because of including the code observation. We can choose any one from the two code–phase ionospheric-free combinations $\mathrm{L}_{\mathrm{P}_1^s\Phi_1^s}^{s}$ and $\mathrm{L}_{\mathrm{P}_2^s\Phi_2^s}^{s}$, to avoid the impact of the more higher measurement noise when using both them. In this paper, the code–phase ionospheric-free combinations $\mathrm{L}_{\mathrm{P}_2^s\Phi_2^s}^{s}$ is used to build a new model for a fast-PPP. Taking into account the ionospheric effects on the dual-frequency phase and code observations, $I_2^s = f_1^2/f_2^2 \cdot I_1^s$, the observation system of the new model can be expressed as:

$$\begin{cases} \Phi_1^s = \rho_r^s + c\cdot\delta\bar{t}_r - c\cdot\delta\bar{t}^s + M_d^s\cdot\delta_{zpd} + M_w^s\cdot\delta_{zpw} - I_1^s + \lambda_1\cdot\bar{N}_1^s + \varepsilon_{\Phi_2^s} \\ \Phi_2^s = \rho_r^s + c\cdot\delta\bar{t}_r - c\cdot\delta\bar{t}^s + M_d^s\cdot\delta_{zpd} + M_w^s\cdot\delta_{zpw} - f_1^2/f_2^2\cdot I_1^s + \lambda_2\cdot\bar{N}_2^s + \varepsilon_{\Phi_2^s} \\ L_{P_2^s\Phi_2^s}^s = \left(P_2^s + \Phi_2^s\right)/2 = \rho_r^s + c\cdot\delta\bar{t}_r - c\cdot\delta\bar{t}^s + M_d^s\cdot\delta_{zpd} + M_w^s\cdot\delta_{zpw} + \lambda_2\cdot\bar{N}_2^s/2 + \varepsilon_{L_{P_2\Phi_2}^s} \\ \Phi_{GF}^s = \Phi_1^s - \Phi_2^s = \left(f_1^2/f_2^2 - 1\right)\cdot I_1^s + \lambda_1\cdot\bar{N}_1^s - \lambda_2\cdot\bar{N}_2^s + \varepsilon_{\Phi_{GF}^s}. \end{cases} \tag{7}$$

If ρ_{r0}^s is the approximate geometric distance between satellite and receiver, then the linearized model of the observation system in Eq. (7) is given as

$$\boldsymbol{y} = \boldsymbol{A}\cdot\boldsymbol{X} + \boldsymbol{\varepsilon_y}, \boldsymbol{\varepsilon_y} \sim \boldsymbol{N}(\boldsymbol{0}, \boldsymbol{\Omega_y}) \tag{8}$$

with

$$\begin{cases} \boldsymbol{y} = \left[\Delta\Phi_1^1 \quad \cdots \quad \Delta\Phi_1^j \quad \Delta\Phi_2^1 \quad \cdots \quad \Delta\Phi_2^j \quad \Delta L_{P_2\Phi_2}^1 \quad \cdots \quad \Delta L_{P_2\Phi_2}^j \quad \Delta\Phi_{GF}^1 \quad \cdots \quad \Delta\Phi_{GF}^j\right]^T \\ \boldsymbol{X} = \left[x \quad y \quad z \quad c\cdot\delta\bar{t}_r \quad \delta_{zpw} \quad I_1^1 \quad \cdots \quad I_1^j \quad \bar{N}_1^1 \quad \cdots \quad \bar{N}_1^j \quad \bar{N}_2^1 \quad \cdots \quad \bar{N}_2^j\right]^T \\ \boldsymbol{A} = \left[\begin{bmatrix} \boldsymbol{e}_3 \\ \boldsymbol{0} \end{bmatrix} \otimes \mathbf{B} \quad \mathbf{C}\otimes\mathbf{I}_j \quad \mathbf{D}\otimes\mathbf{I}_j\right] \end{cases} \tag{9}$$

where $\boldsymbol{y}$ the vector of observed minus computed measurements, $\Delta\Phi_1^s = \Phi_1^s - \rho_{r0}^s + c\cdot\delta\bar{t}^s$, $\Delta\Phi_2^s = \Phi_2^s - \rho_{r0}^s + c\cdot\delta\bar{t}^s$, $\Delta L_{P_2\Phi_2}^s = L_{P_2\Phi_2}^s - \rho_{r0}^s + c\cdot\delta\bar{t}^s$,$\Delta\Phi_{GF}^s = \Phi_{GF}^s - \rho_{r0}^s + c\cdot\delta\bar{t}^s$, $\boldsymbol{X}$ the estimated parameter vector, $\boldsymbol{A}$ the linearization design matrix, $\boldsymbol{\varepsilon_y}$ the system noise, $\boldsymbol{\Omega_y}$ the covariance matrix of the system noise $\boldsymbol{\varepsilon_y}$, '$\otimes$' the Kronecker product, $\mathbf{e}_3$ a 3-dimensional column-vector with all elements as one, $\mathbf{I}_j$ a j-dimensional identity matrix.

The sub-matrices **B**, **C** and **D**, given in Eq. (9), take the following form:

$$\mathbf{B} = \begin{bmatrix} \left(\frac{\partial\rho}{\partial x}\right)^1 & \left(\frac{\partial\rho}{\partial y}\right)^1 & \left(\frac{\partial\rho}{\partial z}\right)^1 & 1 & M_w^1 \\ \vdots & \vdots & \vdots & \vdots & \vdots \\ \left(\frac{\partial\rho}{\partial x}\right)^j & \left(\frac{\partial\rho}{\partial y}\right)^j & \left(\frac{\partial\rho}{\partial z}\right)^j & 1 & M_w^j \end{bmatrix}, \mathbf{C} = \begin{bmatrix} -1 \\ -f_1^2/f_2^2 \\ 0 \\ f_1^2/f_2^2 - 1 \end{bmatrix}, \mathbf{D} = \begin{bmatrix} \lambda_1 & 0 \\ 0 & \lambda_2 \\ 0 & \lambda_2/2 \\ \lambda_1 & -\lambda_2 \end{bmatrix}.$$

The new model is called a MUC model because it adopts some of un-combined observations and can estimate the ionospheric delay. To assess the advantage of the MUC model, assume that code observations P_1 and P_2 have the same accuracy, as well as the carrier phase observations of Φ_1 and Φ_2, namely $\sigma_{P_1} = \sigma_{P_2} = 0.3$ m and $\sigma_{\Phi_1} = \sigma_{\Phi_2} = 0.002$ m. The observation systems of four different PPP models are summarized in Table 1. Among the models, the MUC model has the lowest measurement noise level, and eliminates the orbit error, which is more beneficial for the PPP user to obtain the required accuracy (e.g., less than 10 cm) during a short duration.

In order to down-weight low-elevation satellite observations, an elevation-dependent weight method is used to determine the weights of different observations in PPP data processing (Shen et al. 2009). Then, the variances for the code and carrier phase observations are as follows:

Table 1 Observation system, measurement noise level and estimated atmospheric delay parameter in four PPP models

Method	Observation system	Measurement noise level (m)	Atmospheric delay parameter
UC	P_1, P_2, Φ_1, Φ_2	$\sigma_{P_1} = 0.3$, $\sigma_{P_2} = 0.3$ $\sigma_{\Phi_1} = 0.002$, $\sigma_{\Phi_2} = 0.002$	Tropospheric delay Ionospheric delay
UD	$P_{IF} = \left(f_1^2 \cdot P_1 - f_2^2 \cdot P_2\right)/\left(f_1^2 - f_2^2\right)$ $\Phi_{IF} = \left(f_1^2 \cdot \Phi_1 - f_2^2 \cdot \Phi_2\right)/\left(f_1^2 - f_2^2\right)$	$\sigma_{P_{IF}} = 0.894$, $\sigma_{\Phi_{IF}} = 0.007$	Tropospheric delay
UofC	$L_{P_1\Phi_1} = (P_1 + \Phi_1)/2$ $L_{P_2\Phi_2} = (P_2 + \Phi_2)/2$ $\Phi_{IF} = \left(f_1^2 \cdot \Phi_1 - f_2^2 \cdot \Phi_2\right)/\left(f_1^2 - f_2^2\right)$	$\sigma_{L_{P_1\Phi_1}} = 0.15$, $\sigma_{L_{P_2\Phi_2}} = 0.15$ $\sigma_{\Phi_{IF}} = 0.007$	Tropospheric delay
MUC	Φ_1, Φ_2 $L_{P_2\Phi_2} = (P_2 + \Phi_2)/2$ $\Phi_{GF} = \Phi_1 - \Phi_2$	$\sigma_{\Phi_1} = 0.002$, $\sigma_{\Phi_2} = 0.002$ $\sigma_{L_{P_2\Phi_2}} = 0.15$, $\sigma_{\Phi_{GF}} = 0.003$	Tropospheric delay Ionospheric delay

$$\begin{cases} \sigma_P^2 = \dfrac{\sigma_{P,0}^2}{\sin^2(\theta)} \\ \sigma_\Phi^2 = \dfrac{\sigma_{\Phi,0}^2}{\sin^2(\theta)} \end{cases} \tag{10}$$

where θ is the satellite elevation angle; $\sigma_{P,0}^2$ and $\sigma_{\Phi,0}^2$ are the a priori variance of code and carrier phase observation, respectively.

Moreover, without considering the correlation between code and carrier phase observations, the variance–covariance matrix of the jth satellite observations in the MUC model can be derived using the propagation law of variance and covariance. Hence,

$$\sigma_j^2 = \begin{bmatrix} \sigma_{\Phi_1}^2 & 0 & 0 & \sigma_{\Phi_1}^2 \\ 0 & \sigma_{\Phi_2}^2 & \dfrac{\sigma_{\Phi_2}^2}{2} & -\sigma_{\Phi_2}^2 \\ 0 & \dfrac{\sigma_{\Phi_2}^2}{2} & \dfrac{\sigma_{\Phi_2}^2 + \sigma_{P_2}^2}{4} & -\dfrac{\sigma_{\Phi_2}^2}{2} \\ \sigma_{\Phi_1}^2 & -\sigma_{\Phi_2}^2 & -\dfrac{\sigma_{\Phi_2}^2}{2} & \sigma_{\Phi_1}^2 + \sigma_{\Phi_2}^2 \end{bmatrix}. \tag{11}$$

2.2 Kalman-filtering equation

Kalman-filtering is usually used to estimate the state of the observation system. In this case, the system dynamics can be written as follows:

$$\boldsymbol{X}_{k+1} = \boldsymbol{\Phi}_{k+1,k}\boldsymbol{X}_k + \boldsymbol{w}_k, \quad \boldsymbol{w}_k \sim N(\boldsymbol{\theta}, \boldsymbol{Q}_k) \tag{12}$$

where $\boldsymbol{X}_k$ the state vector, $\boldsymbol{\Phi}_{k+1,k}$ the state transition matrix, $\boldsymbol{w}_k$ the system noise, $\boldsymbol{Q}_k$ the covariance matrix of the system noise $\boldsymbol{w}_k$.

The covariance matrix $\boldsymbol{Q}_k$ reveals the time-varying characteristic of each parameter to be estimated. The MUC model can provide the estimation of the ionospheric delay along the signal path in addition to receiver coordinates, receiver clock, tropospheric delay and phase biases. A random walk process is used to characterize the receiver clock, ionospheric

and tropospheric delay in PPP data processing, while the phase biases are assumed to stay constant. Thus, the covariance matrix $\boldsymbol{Q}_k$ can be expressed as:

$$\boldsymbol{Q}_k = \begin{bmatrix} \underset{3\times3}{q_{\mathrm{p}}\,\Delta t} & \mathbf{0} & \mathbf{0} & \mathbf{0} & \mathbf{0} \\ \mathbf{0} & q_{\mathrm{t_r}}\Delta t & \mathbf{0} & \mathbf{0} & \mathbf{0} \\ \mathbf{0} & \mathbf{0} & q_{\mathrm{trop}}\Delta t & \mathbf{0} & \mathbf{0} \\ \mathbf{0} & \mathbf{0} & \mathbf{0} & \underset{n\times n}{q_{\mathrm{ion}}\,\Delta t} & \mathbf{0} \\ \mathbf{0} & \mathbf{0} & \mathbf{0} & \mathbf{0} & \underset{2n\times 2n}{\mathbf{0}} \end{bmatrix} \tag{13}$$

where Δt the time increment, q_{p} the spectral density of receiver coordinates, which is the identity (or zero) matrix in static (or dynamic) mode, respectively, $q_{\mathrm{t_r}}$ the spectral density of receiver clock, q_{trop} the spectral density of the tropospheric delay, q_{ion} the spectral density of the ionospheric delay.

3 Experiments and result analysis

In this part, we perform static PPP to test the MUC model and compare with the UC, UofC and UD models. Both solutions have been performed over the same 5-day observations data at IGS mana station from June 17 to 21, 2013 (DOY 168–172) and 1-day observations data from 144 IGS stations on June 17, 2013 (DOY 168). The distribution of the stations is shown in Fig. 1. In PPP data processing, the final precise GPS satellite orbits at a sampling interval of 15 min and satellite clock corrections at an interval of 30 s are used (ftp://igsws.unavco.org/pub/gps/). For the Kalman filter, the spectral densities of receiver clock, tropospheric delay and ionospheric delay are set as 1.0×10^{5} m^2/s (El-Mowafy 2009), 7.7×10^{-12} m^2/s (Abdel-Salam and Gao 2003), 1.0×10^{-4} m^2/s (Zhang et al. 2010), respectively. The cut-off elevation angle is set up to 5°.

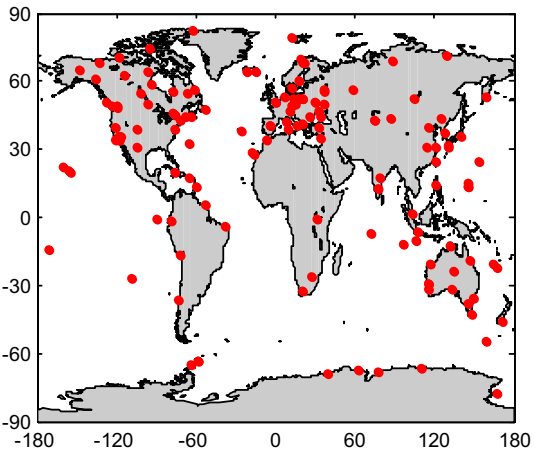

Fig. 1 Distribution of IGS stations

In order to analyze the convergence percentage, convergence time and positioning accuracy of the MUC model, two experiments are conducted. These experiments are as follows:

Experiment I Access the convergence performance of the MUC model. The 5-day observations data at IGS mana station are performed to analyze the convergence time and positioning accuracy. Then, the 1-day observations data from 144 IGS stations are split in every 1, 0.5 and 0.25 h, to get 3456, 6912 and 13,824 group data sets, respectively. We perform the static PPP to analyze the percentages of achieving sub-decimeter level positioning within a relatively short observation period.

Experiment II The 6912 group data sets with 0.5 h observation duration are used to evaluate the positioning performance. We extract the data sets that can both achieve sub-decimeter level positioning based on the MUC and UC models, the MUC and UofC models, as well as the MUC and UD models, to get 3007, 4090 and 1180 group data sets respectively, denoted as A, B and C in the sequel. The convergence times and positioning accuracies for different PPP models are analyzed based on the data sets A, B and C. We analyze the mean bias and standard deviation in the north, east and up components, as well as their 2-dimensional (2D) and 3-dimensional (3D) position for the MUC model, and compare with those of the UC, UofC and UD models.

Note that "convergence" often refers to the positioning accuracy reaching a certain level. In these experiments, the coordinates provided by IGS (ITRF 2008) are used as the true coordinates. When the horizontal position biases between the calculated and the true coordinates are all less than 10 cm from a certain epoch, sub-decimeter level positioning can be achieved. The convergence time refers to the span from the first epoch to a certain epoch from which the horizontal position biases are all less than 10 cm.

The results are as follows:

(1) Experiment I

In this study, we first perform static PPP with real-valued phase-biases based on the 5-day observations data at IGS mana station. Figure 2 shows the positioning accuracies and convergence time for the MUC, UC, UofC and UD models at IGS mana station. After convergence, the position RMS errors of all PPP models are at the sub-centimeter level in the north, east and up. However, there are a few differences in terms of the convergence time. Compared to the UC, UofC and UD models, the MUC model just costs 13.5 min to achieve positioning accuracies within 10 cm in both the north and east components.

In order to analyze the positioning performance of the MUC model during a short observation duration, we perform static PPP with real-valued phase-biases based on 3456, 6912 and 13,824 group data sets, respectively. The percentages of achieving sub-decimeter level positioning are obtained. Figure 3 shows the convergence percentages for the MUC, UC, UofC and UD models for different observation durations. Generally, PPP solution gradually converges to sub-decimeter level with the accumulation of the observations data. As can be seen from Fig. 3, the convergence performance of all PPP models decreases with the reduction of the observation duration, but the MUC model still has a better convergence performance compared with the UC, UofC and UD models. For the 1 h duration observation data sets, a similar convergence percentage of about 86.5 % is obtained for the MUC and UofC models because of the relatively abundant observation data, while the mean convergence time is 18.6 and 19.7 min, respectively. Moreover, compared with the UC and UD models, the convergence percentage for the MUC model is increased by 6.7 and 43.9 %, and the mean convergence time is shortened by 24.1 and 41.9 %, respectively.

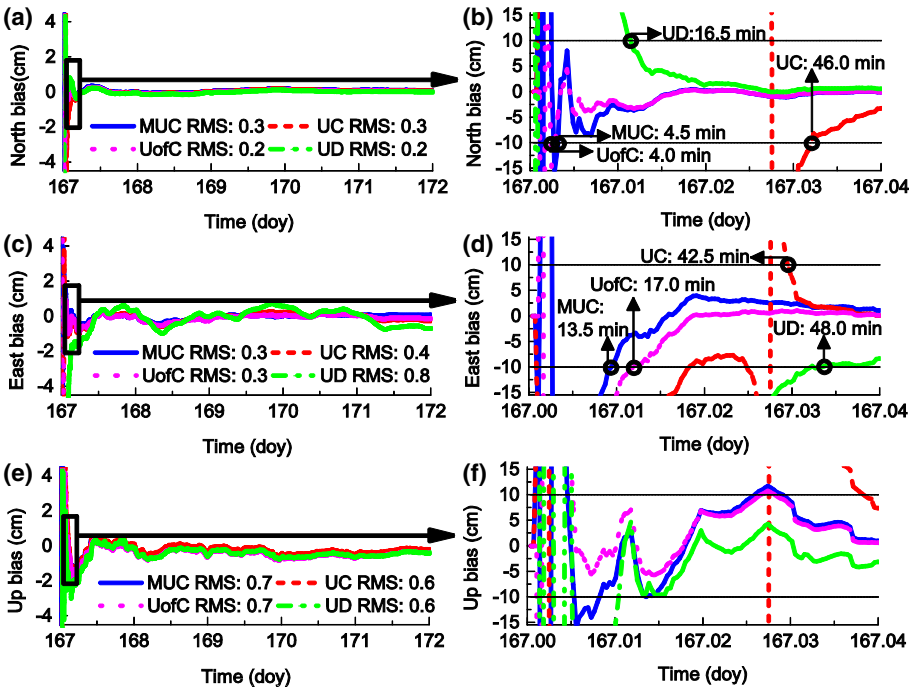

Fig. 2 Position biases for the different PPP models at IGS mana station. **a**, **b** The time series of the north component, **c**, **d** the time series of the east component, **e**, **f** the time series of the up component

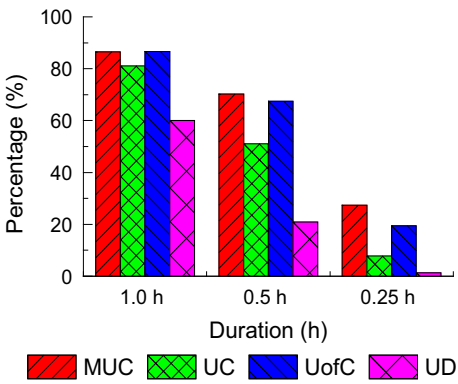

Fig. 3 Percentage of convergence to sub-decimeter level in the horizontal components performed by the MUC, UC, UofC and UD models for the 1.0, 0.5 and 0.25 h duration observation data sets

When the observation time span is short, the estimated parameters are highly-correlated resulting from a small change in the receiver-satellite geometry, which goes against the convergence performance. However, in the MUC model, a new phase–phase geometry-free combination is considered to improve the correlation between the parameter variables over short observation periods. And the MUC model can capture the changing characteristics of atmospheric delays between epochs as constraints to accelerate the filter convergence. These are beneficial to improve the convergence performance. When the observation

duration is reduced to 0.5 h, the convergence percentage of the MUC model is the highest at 70.2 %. Compared with the UC, UofC and UD models, the convergence percentage is increased by 19.2, 2.8 and 49.3 % points, respectively. Furthermore, about 27.4 % of all 13,824 convergence tests can obtain sub-decimeter level positioning after 0.25 h of observation for the MUC model, which is increased by 19.6, 7.9 and 26.1 % points compared with the UC, UofC and UD models. Thus, the MUC model is more beneficial to enhance convergence performance during a short observation duration.

(2) Experiment II

It's well known that for ambiguity-float PPP, it takes about 30–60 min to obtain smaller than 10 cm position error in static mode (Bisnath and Gao 2009; Dawidowicz and Krzan 2014). So this paper focuses on the analysis of the convergence time using the 0.5 h observations data. The mean convergence times of different PPP models are analyzed based on the data sets A, B and C. Figure 4 shows the detailed statistical results of the convergence time of achieving sub-decimeter level positioning in corresponding data sets. In Fig. 4, the box plot is particularly useful for obtaining condensed information about the convergence time, which shows the maximum, minimum, median and quartile values, as well as the average for all the convergence times.

To some extent, the convergence speed suffers from higher measurement noise and orbit error level, so that a longer convergence time is required for the UC model, as shown in Fig. 4a. For the UC model, about half of all 3007 group data can converge to sub-decimeter level within 15.5 min, a quarter of that is less than 11.5 min. When using the MUC model, the convergence time is significantly reduced. There are about half of all the test data sets which can converge to sub-decimeter level within 11.0 min, a quarter of that is less than 8.0 min. And the mean convergence time of the MUC model is 12.1 min, which is shorter by 22.9 % compared with the UC model. These numbers show that the mean convergence time is shorter and more concentrated than that of the UC model. In addition, the statistical results of the convergence time for the MUC and UofC models are as shown in Fig. 4b. The UofC model has a better convergence performance compared with the UC and UD models because of its smaller measurement noise (Zhang et al. 2013b; Zhao et al. 2014). However, the observation system of the UofC model still has a higher measurement noise and orbit error level compared with the MUC model. It can be seen that the mean convergence time of the UofC model is 13.6 min, and only 12.3 min for the MUC model. Therefore, a 9.6 % improvement has been obtained using the MUC model proposed by this paper. Moreover, for the MUC and UofC models, about half of all 4090 group data sets can converge to sub-decimeter level within 11.5 and 13.0 min,

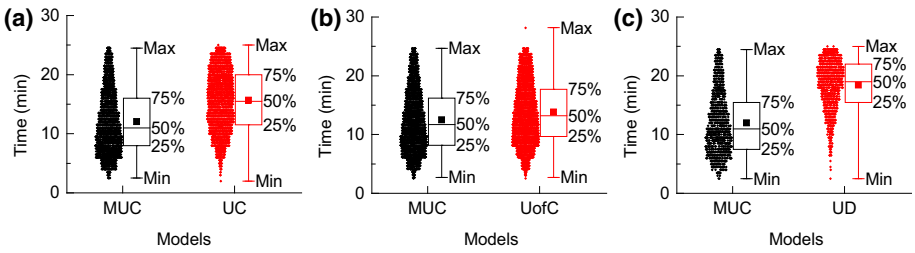

Fig. 4 Statistical results of the convergence time. **a** The results from all data set A with the 0.5 h observation duration, **b** the results from all data set B with the 0.5 h observation duration, **c** the results from all data set C with the 0.5 h observation duration

respectively, and a quarter is less than 8.0 and 9.5 min, respectively. It shows that the convergence speed of the MUC model is faster than that of the UofC model. Among these PPP models, the observation system of the UD model has a highest measurement noise level, resulting in a long convergence time. Compared with the UD model, the mean convergence time of the MUC model is significantly reduced by 35.3 %, as shown in Fig. 4c.

From these results, it can be concluded that the MUC model has a better convergence performance compared with the UC, UofC and UD models. It is more beneficial for the PPP users to quickly obtain sub-decimeter positioning within a short duration.

Further, some preliminary analysis on positioning accuracy has been conducted based on the MUC, UC, UofC and UD models with data sets A, B and C. Figure 5 shows the magnitude distribution of these coordinate biases, where the biases follow normal distributions in the north, east and up components.

The mean bias and standard deviation for data set A, B and C are plotted in Fig. 6. Among the MUC, UC and UofC models, the mean bias shows a satisfactory agreement in both positioning biases. The biases are about 0.5, 0.1, 0.6, 3.7 and 10.0 cm in the north, east, up, 2D and 3D, respectively, which are better than that of the UD model. In addition, the standard deviations for the four models are about 2.4–4.5 cm in both the north and east components, and 10.5–13.9 cm in the up component resulted from the strong correlation between the up component and the tropospheric delay (Li et al. 2010). As can be seen from Fig. 6d–f, the standard deviation for the MUC model is about 2.3 cm in the 2D position and 5.5 cm in the 3D position. Based on the mean and standard deviation (Fig. 6a–f), the positioning accuracy of the MUC model is better than 6.0 cm in the 2D position and less than 16.0 cm in the 3D position. Moreover, the positioning accuracies of the MUC model agree well with those of the UofC model over all test data sets, and these are better than those of the UC and UD models.

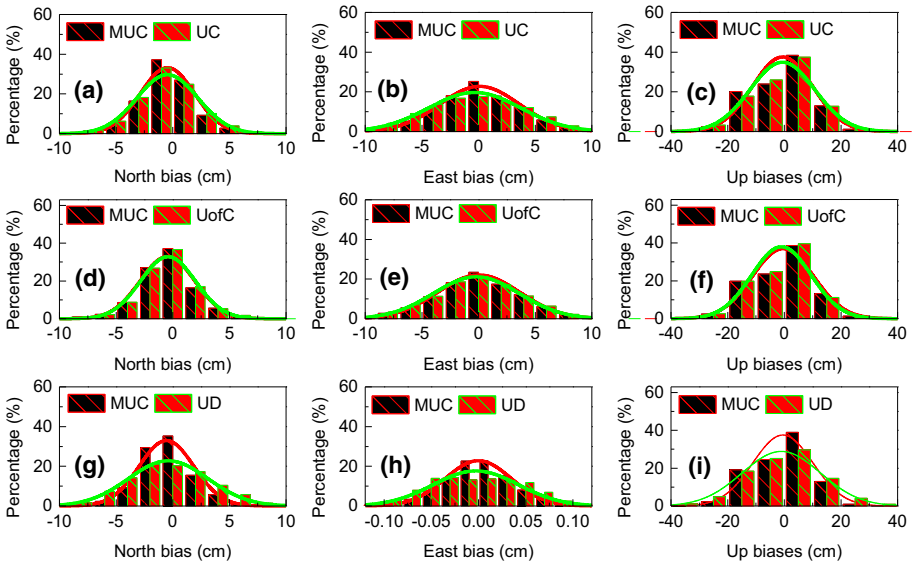

Fig. 5 Distribution of coordinate biases in the north, east and up components for 0.5 h observation duration. **a–c** The results from data set A, **d–f** the results from data set A, **g–i** the results from data set A

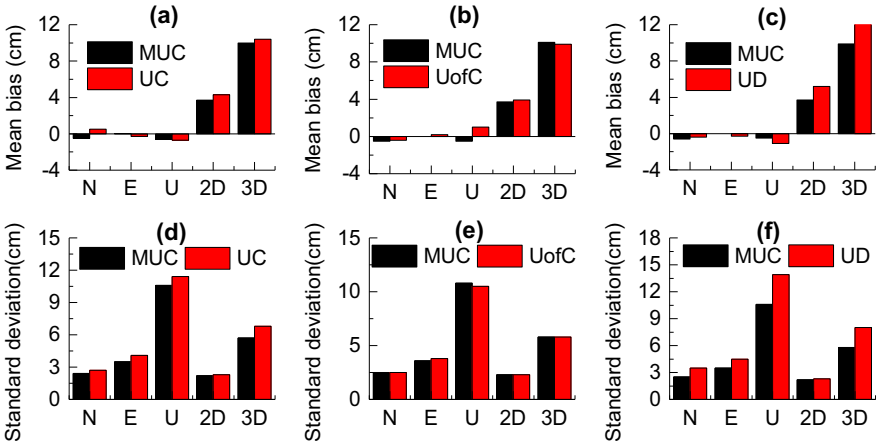

Fig. 6 Comparison between different PPP models in terms of mean bias and standard deviation for data set A (**a**, **d**), data set B (**b**, **e**) and data set C (**c**, **f**) with 0.5 h observation duration (cm)

Due to the low accuracy in up component, we emphatically analyze the accuracy in the 2D position estimate to assess the performance of the MUC model. Figure 7 shows the distribution of the 2D position biases the MUC, UC, UofC and UD models with data sets A, B and C, respectively. From Fig. 7a, it can be seen that the mean 2D position biases of the MUC and UC models are 3.7 and 4.3 cm, respectively. And compared with the UC model, the percentage of the 2D position biases within 0–5 cm is improved by 16.0 % from 65.0 to 75.4 % using the MUC model. It shows that the accuracy in the 2D position is higher than that of the UC model, which is a result of the smaller measurement noise and orbit error level in the observation system of the MUC model. Figure 7b is the results from the data set B based on the MUC and UofC models. It can be seen that a similar mean 2D position bias is obtained for the MUC and UofC model, being 3.7 and 3.9 cm, respectively. Moreover, more than 73.9 % of all 2D position biases are less than 5 cm using the MUC method, which is increased by 3.4 % compared with the UofC model. Because of the higher measurement noise of the observation system for the UD model, the mean 2D position bias is 5.2 cm, while that of the MUC model is smaller, just being 3.7 cm

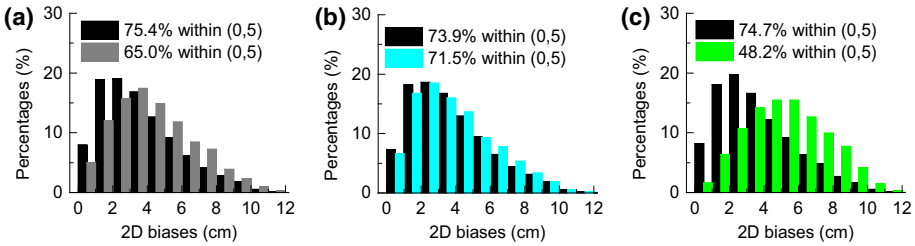

Fig. 7 Distribution of the 2D position biases. **a** The results from the data sets A, *black* shows the 2D biases of the MUC model, *gray* is for that of the UC model; **b** the results from the data sets B, *black* shows the 2D biases of the MUC model, *cyan* is for that of the UofC model, **c** the results from the data sets C, *black* shows the 2D biases of the MUC model, *green* is for that of the UD model. (Color figure online)

(Fig. 7c). Moreover, the percentage of the 2D position biases within 0–5 cm is improved by 55.0 % compared to the UD model.

4 Conclusions

We have proposed a modified un-combined PPP model to accelerate the position convergence. An optimal observation system with minimal measurement noise has been developed. It can capture the changing characteristics of atmospheric delays between epochs as constraints to accelerate the filter convergence. In order to improve the correlation between the parameter variables over short observation periods, the phase–phase geometry-free combinations are used in the observation system. A stochastic model used in Kalman filter estimation has also been presented. Then, the MUC model has been tested and compared with the UC, UofC and UD models. Numerical results indicate that the MUC model has a better convergence performance compared with the UC, UofC and UD models. Especially for a short observation period, such as 0.5 h, the convergence percentage for the MUC model is increased by 19.2, 2.8 and 49.3 % points, respectively, compared with UC, UofC and UD models. For the common convergence parts of all the test data sets, the mean convergence time of the MUC model is shortened by 18.4, 7.2 and 29.5 %, respectively, compared with the UC, UofC and UD models. And the percentage of the 2D position biases within 0–5 cm is increased by 16.0, 3.4 and 55.0 %, respectively. Therefore, the MUC model is more beneficial for the PPP users to quickly obtain positioning accuracies within 10 cm during a short duration.

Acknowledgments This work was partially supported by the National Natural Science Foundation of China (Nos. 41404004, 41474026), Anhui Natural Science Foundation of China (No. 1408085QD72), Fujian Natural Science Foundation of China (No. 2015J01176) and Postdoctoral Science Foundation of Anhui Province of China (No. 2015B044). We also thank the IGS communities for the provision of GPS data and products.

References

Abdel-Salam M, Gao Y (2003) Ambiguity resolution in precise point positioning: preliminary results. In: Proceedings of ION GPS 2003, Portland, pp 1222–1228

Ahmed F, Vaclavovic P, Teferle FN, Dousa J, Bingley R, Laurichesse D (2014) Comparative analysis of real-time precise point positioning zenith total delay estimates. GPS Solut. doi:10.1007/s10291-014-0427-z

Bisnath S, Gao Y (2009) Current state of precise point positioning and future prospects and limitations. In: Sideris MG (ed) Observing our changing earth, international association of geodesy symposia, vol 133. Springer, Berlin, pp 615–623

Cai CS, Gao Y (2013) Modeling and assessment of combined GPS/GLONASS precise point positioning. GPS Solut 17:223–236

Collins P (2008) Isolating and estimating undifferenced GPS integer ambiguities. In: Proceedings of ION NTM 2008, Institute of Navigation, San Diego, California, pp 720–732

Collins P, Bisnath S, Lahaye F, Héroux P (2010) Undifferenced GPS ambiguity resolution using the decoupled clock model and ambiguity datum fixing. Navigation 57(2):123–135

Dawidowicz K, Krzan G (2014) Coordinate estimation accuracy of static precise point positioning using online PPP service, a case study. Acta Geod Geophys 49:37–55

Defraigne P, Baire Q (2011) Combining GPS and GLONASS for time and frequency transfer. Adv Space Res 47(2):265–275

El-Mowafy A (2009) Alternative postprocessing relative positioning approach based on precise point positioning. J Surv Eng 135(2):56–65

Gao Y, Shen X (2001) Improving ambiguity convergence in carrier phase-based precise point positioning. In: Proceedings of ION GPS 2001, Salt Lake City, UT, pp 1532–1539
Ge M, Gendt G, Rothacher M, Shi C, Liu J (2008) Resolution of GPS carrier-phase ambiguities in precise point positioning (PPP) with daily observations. J Geod 82(7):389–399
Geng JH, Teferle F, Shi C, Meng X, Dodson AH, Liu J (2009) Ambiguity resolution in precise point positioning with hourly data. GPS Solut 13(4):263–270
Geng J, Teferle FN, Meng X, Dodson AH (2011) Towards ppp-rtk: ambiguity resolution in real-time precise point positioning. Adv Space Res 47(10):1664–1673
Kouba J, Heroux P (2001) Precise point positioning using IGS orbit and clock products. GPS Solut 5(2):12–28
Laurichesse D, Mercier F, Berthias JP, Broca P, Cerri L (2009) Integer ambiguity resolution on undifferenced GPS phase measurements and its application to PPP and satellite precise orbit determination. Navigation 56(2):135–149
Li P, Zhang XH (2014) Integrating GPS and GLONASS to accelerate convergence and initialization times of precise point positioning. GPS Solut 18:461–471
Li BF, Feng YM, Shen YZ, Wang C (2010) Geometry-specified troposphere decorrelation for subcentimeter real-time kinematic solutions over long baselines. J Geophys Res Solid Earth. doi:10.1029/2010JB007549
Li X, Ge M, Zhang H, Wickert J (2013) A method for improving uncalibrated phase delay estimation and ambiguity-fixing in real-time precise point positioning. J Geod 87(5):405–416
Li L, Long SC, Li HJ, Zhang LY (2014a) Precise point positioning based on reference stations augmentation information. Acta Geod Cartogr Sin 43(5):481–485
Li T, Wang JL, Laurichesse D (2014b) Modeling and quality control for reliable precise point positioning integer ambiguity resolution with GNSS modernization. GPS Solut 18:429–442
Moreno B, Rodriguez-Caderot G, De Lacy C (2014) Multi-frequency algorithms for precise point positioning: MAP3. GPS Solut 18:355–364
Shen Y, Li B, Xu G (2009) Simplified equivalent multiple baseline solutions with elevation-dependent weights. GPS Solut 13(3):165–171
Shi JB, Xu CQ, Guo JM, Gao Y (2014) Local troposphere augmentation for real-time precise point positioning. Earth Planets Space 66(1):1–13
Teunissen PJG, Kleusberg A (1996) GPS observation equations and positioning concepts. In: Kleusberg A, Teunissen PJG (eds) GPS for geodesy. Springer, Berlin, pp 175–217
Wen Z, Henkel P, Günther C (2015) Precise point positioning with partial ambiguity fixing and optimal subset selection. In: International association of geodesy symposia. Springer, Berlin. doi:10.1007/1345_2015_110
Xu P, Shi C, Fang R, Liu J, Niu X, Zhang Q, Yanagidani T (2013) High-rate precise point positioning (PPP) to measure seismic wave motions: an experimental comparison of GPS PPP with inertial measurement units. J Geod 87(4):361–372
Zhang BC, Ou JK, Yuan YB, Zhong SM (2010) Precise point positioning algorithm based on original dual-frequency GPS code and carrier-phase observations and its application. Acta Geod Cartogr Sin 39(5):478–483
Zhang BC, Teunissen PJ, Odijk D, Ou JK, Jiang ZW (2012) Rapid integer ambiguity-fixing in precise point positioning. Chin J Geophys 55(7):2203–2211
Zhang XH, Li P, Zuo X (2013a) Kinematic precise orbit determination based on ambiguity-fixed PPP. Geomat Inf Sci Wuhan Univ 38(9):1009–1013
Zhang XH, Zuo X, Li P (2013b) Mathematical model and performance comparison between ionosphere-free combined and uncombined precise point positioning. Geomat Inf Sci Wuhan Univ 38(5):561–565
Zhao XW, Wang SL, Deng J, Liu C (2014) Performance analysis of four function models for precise point positioning. J Hefei Univ Technol 27(6):751–756
Zhao XW, Wang SL, Liu C, Ou JK, Yu XX (2016) Assessing the performance of multi-GNSS precise point positioning in Asia-Pacific region. Surv Rev. doi:10.1080/00396265.2016.1151576
Zumbeger JF, Heflin MB, Jefferson DC, Watkins MM, Webb FH (1997) Precise point positioning for the efficient and robust analysis of GPS data from large networks. J Geophys Res 102(B3):5005–5017